Available online at www.sciencedirect.com
SCIENCE DIRECT®
Journal of the Mechanics and Physics of Solids
53 (2005) 2206–2230
JOURNAL OF THE MECHANICS AND PHYSICS OF SOLIDS
www.elsevier.com/locate/jmps

Dynamic compressive strength properties of aluminium foams. Part II—'shock' theory and comparison with experimental data and numerical models

P.J. Tan, S.R. Reid*, J.J. Harrigan, Z. Zou, S. Li

School of Mechanical, Aerospace and Civil Engineering, The University of Manchester, P.O. Box 88, Sackville Street, Manchester M60 1QD, UK

Received 25 October 2004; received in revised form 16 May 2005; accepted 17 May 2005

Abstract

One-dimensional 'steady-shock' models based on a rate-independent, rigid, perfectly-plastic, locking (*r-p-p-l*) idealisation of the quasi-static stress–strain curves for aluminium foams are proposed for two different impact scenarios to provide a first-order understanding of the dynamic compaction process. A thermo-mechanical approach is used in the formulation of their governing equations. Predictions by the models are compared with experimental data presented in the companion paper (Part I) and with the results of finite-element simulations of two-dimensional Voronoi honeycombs.

A kinematic existence condition for continuing 'shock' propagation in aluminium foams is established using thermodynamics arguments and its predictions compare well with the experimental data. The thermodynamics highlight the incorrect application of the global energy balance approach to describe 'shock' propagation in cellular solids which appears in some current literature.

Keywords: Shock waves; Foams; Voronoi structure; Inertia effects; Energy absorption

*Corresponding author. Tel.: +44 0161 200 3848; fax: +44 0161 200 3849.
E-mail address: steve.reid@manchester.ac.uk (S.R. Reid).

0022-5096/$ - see front matter © 2005 Elsevier Ltd. All rights reserved.
doi:10.1016/j.jmps.2005.05.003

1. Introduction

The results of an extensive experimental investigation into the dynamic uniaxial compressive response of closed-cell Hydro/Cymat aluminium alloy foams to impact loading are presented in the companion paper by Tan et al. (2005), hereinafter referred to as Part I. It was shown that a foam specimen shortens by the accumulation of discrete, non-contiguous bands of crushed cells when it is compressed dynamically at a sub-critical velocity. However, beyond a critical impact velocity of approximately $108\,\mathrm{ms}^{-1}$ (for the *small* cell specimens) and $42\,\mathrm{ms}^{-1}$ (for the *large* cell specimens), cell crushing occurs sequentially, in a planar manner, along the axis of the specimen from the impact end towards the distal end, and the crushing wave front exhibits 'shock-type' characteristics, i.e. the particle velocity and the deformation gradient (strain) in the specimen suffer finite jumps across the crush front. This paper presents the results of a one-dimensional (1D) 'steady-shock' model which explains some of the qualitative and quantitative features of the formation and the propagation of 'steady-shock' or compaction/consolidation waves (see footnote 4 in Part I) in aluminium foams subjected to impact loading at super-critical velocities. The mathematical techniques used are not original, being familiar to fluid mechanicists and shock physicists, but their application to metal foams provides some new insights.

Structural 'shock' waves are known to provide a useful model for the high velocity progressive crushing behaviour of cellular structures such as those composed of rings/tubes and man-made honeycombs (Reid et al., 1983, 1993; Reid and Reddy, 1983; Reid and Bell, 1984; Reddy et al., 1991). Similarly, a 'shock' model based on a rigid, perfectly-plastic, locking (*r-p-p-l*) idealisation of the quasi-static stress–strain curves of cellular materials can be used to account, via a continuum approximation, for the dominant inertial effects operating at the scale of their cell structure. These studies have been summarised in several publications by the authors (for example Harrigan et al., 1998a,b, 1999, 2005). Use of this simplified constitutive equation has focussed on those dynamic effects that are generally produced in a material/structure with Type-I properties (Calladine and English, 1984), i.e. arising from 'shock' wave generation generally attributed to constitutive laws with a concave upwards plastic loading path (Reid et al., 1993). In testing various materials and structures, there is also evidence, to a greater or lesser extent, that there is some Type-II structural response (Harrigan et al., 1998a, 1999; 2005). This is associated with the *initiation* of deformation in an impact (non-zero initial velocity) process. In all of these previous studies, the formulation of the kinematics and kinetics were based only on jump conditions associated with the conservation of mass and momentum across the 'shock' front. In this paper, a detailed analysis is presented incorporating energy arguments as well. These draw attention to certain issues that are usually treated somewhat superficially, if not incorrectly, in previous work on cellular solids, specifically with regard to the energy absorbed at the 'shock' front.

The method of characteristics is first used to analyse the propagation of plane irrotational compressive-stress waves in a 1D foam 'rod' having a general stress–strain relation with linear elastic and concave-upwards plastic loading paths

(Hanssen, 2002) in Section 2. The emphasis is on explaining the possible occurrence and the conditions leading to the formation of 'shock' waves. In Section 3 the basic jump conditions for the dependent variables across a 'steady-shock' front are stated. To obtain closed-form solution, an *r-p-p-l* idealisation of the stress–strain curve for the 1D foam rod is then adopted and the equation of motion for a plane surface of strong stress discontinuity (or 'shock' wave) propagating in the rod is formulated. Two different impact scenarios are considered: in the first, a foam rod strikes a rigid stationary target and, in the other, a rigid mass strikes a stationary foam rod supported by a rigid surface. Both impact scenarios are possible test configurations for the direct-impact testing technique described in Part I and relate to the two principal modes of the application of metal foams to impact energy absorption. The kinematic existence condition for continuing/propagating 'shock' compaction in the aluminium foams is also established. Comparisons are made between the 'shock' theory, the experimental data and the results of finite element simulations of two-dimensional (2D) Voronoi honeycombs. The limitations of the 'steady-shock' model generally are discussed. In conclusion, the apparently incorrect use of an energy balance equation in Ashby et al. (2000) and Lu and Yu (2003) to formulate governing equation of motion for 'steady-shock' propagation in cellular solids are also discussed.

2. Basic equations

Consider a circular cylindrical foam 'rod' of unit cross sectional area with generators in the X-direction bounded by the surfaces of particles which in their undeformed position lie in the planes $X = 0$ and $X = l_o$. The rod is assumed to be initially uniform and homogeneous in all those properties associated with the principal y-direction of a typical foam panel studied in Part I. In common with other studies on 'steady-shock' propagation in cellular solids (see Reid and Peng, 1997 and Ashby et al., 2000), the usual notion of a continuum is assumed to hold throughout. Suppose that a system of compressive stress waves is generated by normal forces applied to the plane boundary ($X = 0$) at $t = 0$ as depicted in Fig. 1. The governing

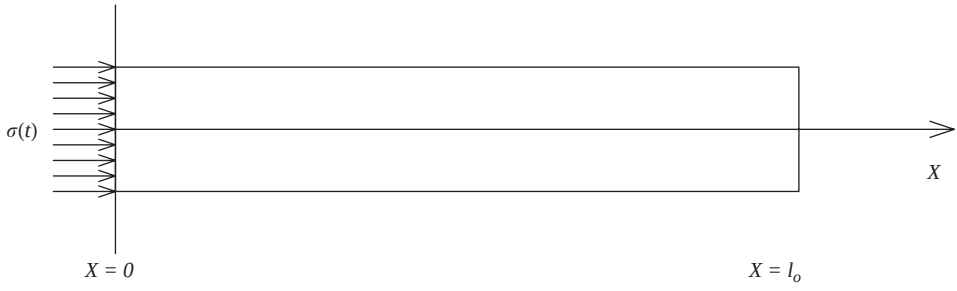

Fig. 1. Coordinate system.

equations are expressed in terms of Lagrangian co-ordinates and engineering stress and strain definitions are adopted. The independent variables are X and t; and the dependent variables are axial displacement u, velocity v, uniaxial compressive strain ε and nominal compressive stress σ, all functions of X and t. Here, and in the rest of the paper, all stresses and strains are treated as positive in compression.

The single material co-ordinate $X \in [0, l_o]$ describes the 1D foam rod so that the position of a typical particle is given by

$$x = x(X, t), \tag{1}$$

where x is the position of the particle at time t which was at position X in the undeformed configuration. The displacement u, velocity v, and compressive strain ε are defined as

$$u(X, t) = x(X, t) - X, \tag{2}$$

$$v = x_{,t} = u_{,t} \tag{3}$$

and

$$\varepsilon = -u_{,X}, \tag{4}$$

where the subscripts $,X$ and $,t$ indicate partial differentiation. The equations of kinematic compatibility, mass conservation and linear momentum are

$$\varepsilon_{,t} + v_{,X} = 0, \tag{5}$$

$$\rho(1 - \varepsilon) = \rho_o, \quad \text{and} \tag{6}$$

$$\frac{\mathrm{d}}{\mathrm{d}t}\int_a^b \rho_o v \,\mathrm{d}X = \int_a^b f \,\mathrm{d}X - \sigma(X, t)\Big|_{X=a}^{X=b}, \tag{7}$$

where ρ and ρ_o are the current and initial densities, respectively; f is the body force per unit volume and the sub-interval $[a, b]$ satisfies $0 \leqslant a < b \leqslant l_o$ at all times. If $v_{,t}$ and $\sigma_{,X}$ exist and a and b were arbitrary, the local form of Eq. (7) is

$$\rho_o v_{,t} = f - \sigma_{,X}. \tag{8}$$

The three likely contributions to the 'rate-sensitive' material response of a cellular solid, viz. compression of the trapped gas (this applies only to cellular solids with closed-cells); strain rate sensitivity of the material of the cell wall which is dependent on thermal activation or dislocation drag processes; and, inertial rate sensitivity due to the inertia of the individual cell walls, are separately discussed in Part I. It was established there that contributions from the compression of trapped gas are negligibly small. Likewise, the aluminium cell wall material was also shown to be strain-rate insensitive. Hence, a time-independent, constitutive equation of the form

$$\sigma = g(\varepsilon) \tag{9}$$

could be used here to describe the uniaxial compressive stress state in the foam rod. For consistency with the strain-hardening model for aluminium foams developed by

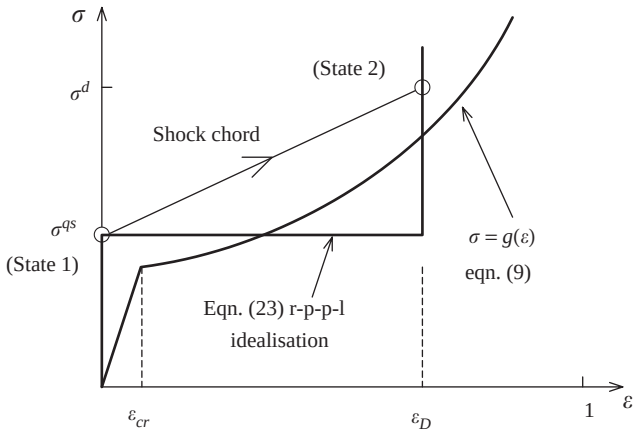

Fig. 2. Nominal stress–strain curve and its idealisation.

Hanssen et al. (2002) for uniaxial and hydrostatic loading conditions, the function g is assumed to possess the following properties:

(i) $\mathrm{d}g/\mathrm{d}\varepsilon > 0$ for every ε in $(\varepsilon_{\mathrm{cr}}, 1)$, and
(ii) $\mathrm{d}^2 g/\mathrm{d}\varepsilon^2 > 0$ in the same interval.

Hence, g is a strictly monotonic increasing function in $[\varepsilon_{\mathrm{cr}}, 1]$ and concave upwards as depicted in Fig. 2.

Combining Eqs. (8) and (9), and ignoring body forces, gives

$$v_{,t} = -c^2(\varepsilon)\,\varepsilon_{,X}, \tag{10}$$

where $c^2(\varepsilon) = (\mathrm{d}\sigma/\mathrm{d}\varepsilon)/\rho_{\mathrm{o}}$. The characteristic analysis of Eqs. (5) and (10) was given by Hopkins (1968) and so the results are simply summarised below:

- On the $C+$ characteristics, given by $\mathrm{d}X/\mathrm{d}t = +c(\varepsilon)$, the $C+$ invariant, $R_1 = u_{,t} + \int_0^{\varepsilon} c(\varepsilon)\,\mathrm{d}\varepsilon$, is constant, and
- on the $C-$ characteristics, given by $\mathrm{d}X/\mathrm{d}t = -c(\varepsilon)$, the $C-$ invariant, $R_2 = u_{,t} - \int_0^{\varepsilon} c(\varepsilon)\,\mathrm{d}\varepsilon$, is constant, where R_1 and R_2 are the Riemann invariants.

It is easily verified that $u_{,t}$ and $\int_0^{\varepsilon} c(\varepsilon)\,\mathrm{d}\varepsilon$ are separately constant on each $C+$ characteristic, and

$$v = u_{,t} = \int_0^{\varepsilon} c(\varepsilon)\,\mathrm{d}\varepsilon. \tag{11}$$

Since $\mathrm{d}c/\mathrm{d}\varepsilon > 0$ (Eq. (9)), this means that stress increment ($\Delta\sigma > 0$) from a plastic stress level $\sigma(0, t_1)$ is eventually overtaken by a second stress increment from a higher stress level $\sigma(0, t_1 + \Delta t_1)$ at the point (Morland, 1959; Hopkins, 1968)

$$X = c_1^2/(\mathrm{d}c_1/\mathrm{d}t_1), \quad t = t_1 + c_1/(\mathrm{d}c_1/\mathrm{d}t_1) \tag{12}$$

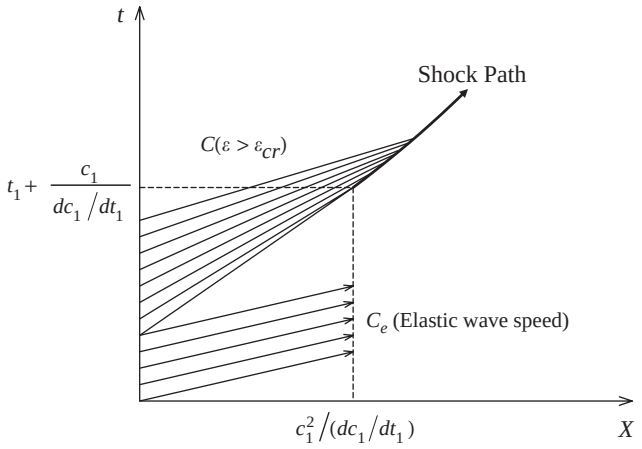

Fig. 3. Characteristic diagram of a simple wave system generated by a smooth and continuous loading force pulse.

in the X-t plane where $c_1 = c(\varepsilon_1)$. This is shown in Fig. 3. Thereafter, the continuous wave solution breaks down and the analysis must proceed with the propagation of a discontinuity. Note that important issues such as the reflection of stress waves from the free or fixed end of the finite rod, which involves complicated interactions between the loading and unloading, elastic and plastic waves (see, for example, Morland, 1959), have not been addressed here. Finally, it should also be noted that if an instantaneous velocity V_i is imposed on the plane boundary ($X = 0$) at $t = 0$, instead of the normal forces prescribed above, the $C+$ characteristics from the plane boundary ($X = 0$) will intersect immediately with those of the foam rod, leading to the immediate formation of a 'shock' moving with a velocity $V_s(< V_i)$.

3. 1D 'shock' models

The propagation of a plane surface of strong stress discontinuity in a 1D foam rod is now considered. First, the basic jump conditions, or the dynamical conditions of compatibility, across a 'shock' front are stated.

3.1. Basic jump conditions and 'shock' interactions

Assume that a 'surface' of strong stress discontinuity (or a 'shock' front) is currently at the material point $X_s = X_s(t)$ and moving at a Lagrangian wave speed of

$$V_s = \mathrm{d}X_s/\mathrm{d}t. \tag{13}$$

Displacement continuity across the 'shock' is expressed, by Hadamard's Lemma,[1] as

$$\mathrm{d}[u]/\mathrm{d}t = [u_{,t}] + V_{\mathrm{s}}[u_{,X}] = [v] - V_{\mathrm{s}}[\varepsilon] = 0. \tag{14}$$

The symbol $[h] \equiv h^{-} - h^{+}$ denotes a jump in the dependent variable, say h, across the 'shock' front where superscripts $-$ and $+$ denote the region immediately behind and just ahead of the 'shock', respectively. If $u_{,t}$ is continuous everywhere except at X_{s}, Eq. (7) gives (Bland, 1988)

$$[\sigma] - \rho_{\mathrm{o}} V_{\mathrm{s}}[v] = 0. \tag{15}$$

For a thermodynamic system, the first law asserts that (Ericksen, 1991; Eringen and Şuhubi, 1974)

$$\begin{aligned}\frac{\mathrm{d}}{\mathrm{d}t}(E_{\mathrm{k}} + E_{\mathrm{U}}) = (H - Q) + \mathrm{P}_{\mathrm{ext}} \Leftrightarrow \frac{\mathrm{d}}{\mathrm{d}t}\left(\int_a^b \rho_{\mathrm{o}}\left(\frac{1}{2}v^2 + U\right)\mathrm{d}X\right)\\ = \left(\int_a^b \rho r\,\mathrm{d}X - q\Big|_{X=a}^{X=b}\right)\\ + \left(\int_a^b fv\,\mathrm{d}X - \sigma v\Big|_{X=a}^{X=b}\right),\end{aligned} \tag{16}$$

where $\mathrm{d}(E_{\mathrm{k}} + E_{\mathrm{U}})/\mathrm{d}t$ is the rate of increase of kinetic plus internal energies (per unit reference area), respectively; U is internal energy per unit mass; q is the X-component of the heat flux vector; and r is the heat source per unit mass of specimen. If $u_{,t}$ and $U_{,t}$ are continuous everywhere except at X_{s}, assuming no heat is generated within the specimen so that $\int_a^b \rho\, r\,\mathrm{d}X = 0$ and ignoring body force, Eq. (16) gives (Bland, 1988)

$$\rho_{\mathrm{o}} V_{\mathrm{s}}[v^2/2 + U] - [\sigma v + q] = 0. \tag{17}$$

The jump conditions in Eqs. (14), (15) and (17) express the fact that the flux of mass, momentum and energy, respectively, must remain continuous across the 'shock' front, whilst the stress, density and internal energy need not be. In a similar manner, the second law of thermodynamics yields the inequality (Ericksen, 1991)

$$V_{\mathrm{s}}[\eta] \geqslant [q/\theta], \tag{18}$$

where η is the specific entropy (or entropy per unit mass) and θ the absolute temperature.

Across the 'shock' front, the jump in the compressive stress is found by eliminating V_{s} between Eqs. (14) and (15) to be

$$[\sigma] = -\rho_{\mathrm{o}}[u_{,t}]^2/[u_{,X}] = \rho_{\mathrm{o}}[v]^2/[\varepsilon] \tag{19}$$

and the 'shock' wave speed is found by eliminating $[v]$ to be

$$V_{\mathrm{s}} = \sqrt{[\sigma]/\rho_{\mathrm{o}}[\varepsilon]}. \tag{20}$$

[1] See Eringen and Şuhubi (1974) for a statement and proof of Hadamard's Lemma.

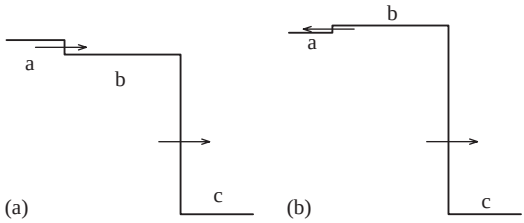

Fig. 4. Situation before (a) and after (b) interaction between a plastic wavelet and the main 'shock' front.

If $V_s \geqslant c_e$ (the elastic wave speed in the foam 'rod' is estimated in Part I), a plastic 'shock' wave propagates into a region of material which is initially undeformed; otherwise, an elastic wave precedes the plastic 'shock' wave. Treating each stress-wave profile as a series of small continuous steps with a constant wave velocity (see Morland, 1959), a plastic loading wavelet will eventually catches up with the main 'shock' front because of the upward curvature of the plastic stress–strain loading path (Eq. (9). This plastic loading wavelet is generated by the compression of the densified cells which, although having limited compressibility, still occurs behind the 'shock' front. The increase in particle velocity across a 'shock' separating two states, viz. '−' and '+', is given by Eqs. (6) and (19) to be

$$[v]_{\to +} = \sqrt{(\sigma^- - \sigma^+)(1/\rho^+ - 1/\rho^-)}. \tag{21}$$

Interaction between the plastic loading wavelet, moving from states '*a*' to '*b*', and the main 'shock' front, moving from states '*b*' to '*c*', is not equivalent to a single 'shock' transition from '*a*' to '*c*', as is evident from a mismatch in their particle velocity where (see Fig. 4)

$$[v]_{a\to c} < [v]_{b\to c} + [v]_{a\to b}. \tag{22}$$

The correct matching of particle velocity can only be achieved by introducing an elastic unloading wave, moving from states '*b*' to '*a*' after interaction. This unloading wave is then reversed by the next oncoming plastic wavelet, and the entire interaction cycle is repeated (Morland, 1959). In simple qualitative terms, this means that the 'shock' wave gradually built-up from behind and with increasing strength its velocity increases. To circumvent the need to consider complicated 'shock' interactions, such as the one just described above, an *r-p-p-l* idealisation of the stress–strain curve for the foam rod will be proposed in Eq. (23).

3.2. Impact of a foam rod against a rigid target

3.2.1. Equation of motion

Consider a foam rod of unit area travelling at a speed of $V_i (< c_e)$ until it strikes squarely a pressure bar at time $t = 0$ as depicted in Fig. 5. The frame of reference is fixed at the proximal (impact) end of the rod at $t = 0$. At $t > 0$ 'shock' compaction of the material occurs at the point $x(X_s, t)$, with the portion of the rod l remaining rigid.

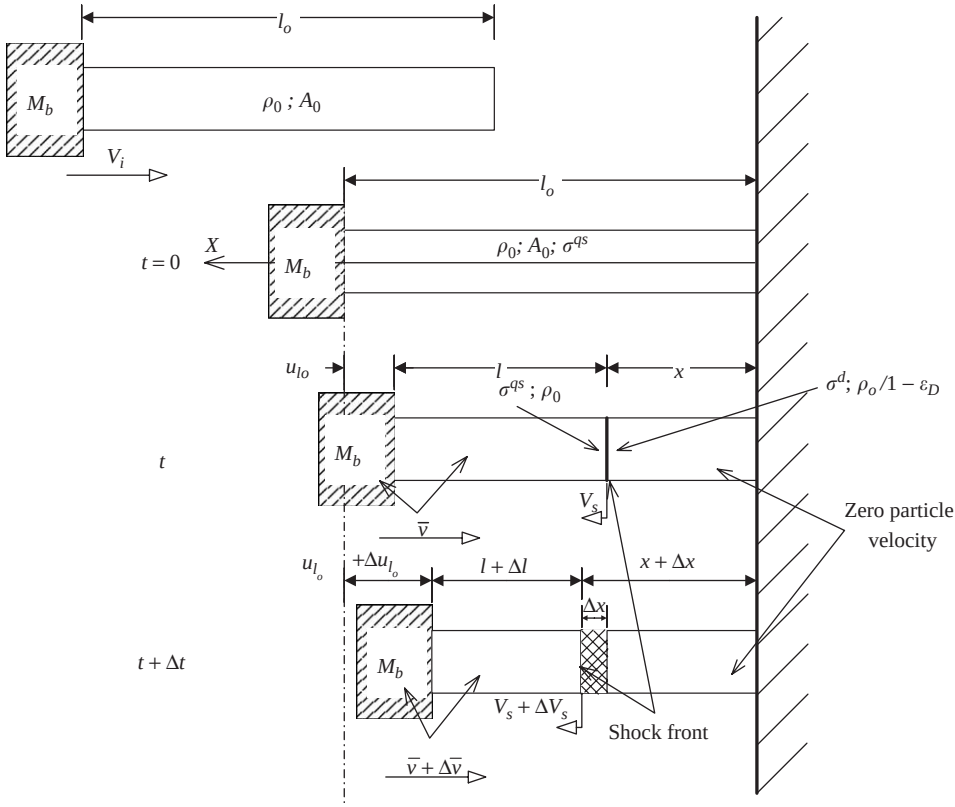

Fig. 5. Parameters defining the 'shock' model for the impact of a foam rod against a rigid stationary target.

In common with the theme of designing with foams for impact energy absorption, and to obtain closed-form solution of the problem, a simple rate-independent *r-p-p-l* idealisation of the stress–strain curve for the foam rod, viz.

$$g(\varepsilon) = \begin{cases} \sigma^{\mathrm{qs}} & 0 \leqslant \varepsilon < \varepsilon_{\mathrm{D}}, \\ +\infty & \varepsilon = \varepsilon_{\mathrm{D}} \end{cases} \tag{23}$$

is adopted here where the superscript qs denotes quasi-static values (see Fig. 2). The response of the material in the densification regime, i.e. $\varepsilon > \varepsilon_{\mathrm{D}}$ (densification strain), is of lesser intrinsic interest in energy absorption applications and, therefore, a locking material assumption at ε_{D} suffices. Although Eq. (23) is no longer strictly monotonic increasing in $[0, \varepsilon_{\mathrm{D}})$, its concave-upwards characteristic makes possible the existence of 'shock' waves. The locking assumption does not permit wave reflections or 'shock' interactions. Its initial rigid response also requires an instantaneous jump in stress from 0 to σ^{qs} in the rod on compression. This implies

that an elastic loading wave travels the length of the rod at an infinite velocity which, given that the elastic wave speed C_e is at least an order of magnitude higher than the impact velocity V_i (see Part I), is not physically unreasonable.

The conditions immediately behind and just ahead of the 'shock' are as follows:

$$\textit{Behind 'shock' front}: \quad v^- = 0,\ \varepsilon^- = \varepsilon_D,\ \sigma^- = \sigma^d,\ \rho^- = \rho_o/(1-\varepsilon_D) \text{ and} \tag{24}$$

$$\textit{Ahead of 'shock' front}: \quad v^+ = \bar{v},\ \varepsilon^+ = 0,\ \sigma^+ = \sigma^{qs},\ \rho^+ = \rho_o. \tag{25}$$

Here, the superscript d denotes dynamic values. Substituting these conditions into Eq. (19) gives the 'shock' relation

$$\sigma^d = \sigma^{qs} + \rho_o \bar{v}^2/\varepsilon_D, \tag{26}$$

which has to be satisfied at all times. Let u_{l_o} ($\equiv |u(l_o, t)|$) be the displacement of the distal end of the foam rod at time t and from geometry (see Fig. 5)

$$l = l_o - u_{l_o} - x \tag{27}$$

and so

$$\dot{l} = \mathrm{d}l/\mathrm{d}t = -(\dot{x} + \dot{u}_{l_o}) = -\dot{u}_{l_o}/\varepsilon_D = -\bar{v}/\varepsilon_D, \tag{28}$$

where $\varepsilon_D = u_{l_o}/(u_{l_o} + x)$.

From Eqs. (14) and (15), it is not difficult to show that

$$[\sigma \cdot v] = (\sigma^- + \sigma^+)V_s[\varepsilon]/2 + \rho_o V_s[v^2]/2. \tag{29}$$

The dynamic compaction process occurs so quickly that the foam rod can be assumed to be non-heat conducting wherein q is identically zero. Substituting Eq. (29) into (17), and setting $[q] = 0$, gives

$$[\rho_o U] - (\sigma^- + \sigma^+)[\varepsilon]/2 = 0, \tag{30}$$

the familiar Rankine–Hugoniot equation. If the straight line (or Rayleigh line) joining the states in front of, and behind, the 'shock', in the stress–strain plane, is defined as the 'shock' chord, then Eq. (30) implies that the change in internal energy per unit reference volume is the area under the 'shock' chord in the closed interval $[\varepsilon^+, \varepsilon^-]$. Thus, the increase in internal energy when an element of length Δl is compacted to $\Delta x = \Delta l(1-\varepsilon_D)$ at the 'shock' front in the time interval t to $t + \Delta t$ is

$$\Delta E_U = E_U(t + \Delta t) - E_U(t) = \tfrac{1}{2}(\sigma^d + \sigma^{qs})\varepsilon_D \Delta l. \tag{31}$$

Over the same time interval, the change in kinetic energy of the undeformed rod, ahead of the 'shock', as it changes velocity from $\bar{v}$ to $\bar{v} + \Delta\bar{v}$ is

$$\Delta E_k = E_k(t + \Delta t) - E_k(t) = \tfrac{1}{2}\{2\bar{v}(M_b + \rho_o l)\Delta\bar{v} + \rho_o \bar{v}^2 \Delta l\} + O(\Delta\bar{v}^2, \Delta l \Delta\bar{v}, \Delta l \Delta\bar{v}^2). \tag{32}$$

If the 'shock' compaction process leaves State 1 at time t and arrives at State 2 at time $t + \Delta t$, then integrating Eq. (16), assuming an isolated system wherein

$\delta Q = \delta P_{\text{ext}} = 0$, gives

$$(E_{\text{k}} + E_{\text{U}})_2 - (E_{\text{k}} + E_{\text{U}})_1 = 0. \tag{33}$$

From Eqs. (28), (31) and (32) and ignoring all higher order quantities of small terms, dividing by Δt and taking the limit $\Delta t \to 0$, Eq. (33) gives the equation of motion of the distal end of the foam rod as

$$\left\{(1 + M_{\text{r}}) - u_{l_{\text{o}}}/\varepsilon_{\text{D}} l_{\text{o}}\right\} \text{d}\bar{v}/\text{d}t = -\sigma^{\text{qs}}/\rho_{\text{o}} l_{\text{o}}, \tag{34}$$

where the mass ratio $M_{\text{r}} \equiv M_{\text{b}}/\rho_{\text{o}} l_{\text{o}}$. An equivalent kinematic approach in which considerations are given only to the purely mechanical conditions at the 'shock' front, viz. Eqs. (7), (19), (20), (27) and (28), was previously used by Reid and Peng (1997) to derive Eq. (34). This last equation is easily integrated with the initial condition $\bar{v}(u_{l_{\text{o}}} = 0) = V_{\text{i}}$ to give

$$\bar{v} = \text{d}u_{l_{\text{o}}}/\text{d}t = \left\{V_{\text{i}}^2 + 2\sigma^{\text{qs}}\varepsilon_{\text{D}} \ln(1 - u_{l_{\text{o}}}/(1 + M_{\text{r}})\varepsilon_{\text{D}} l_{\text{o}})/\rho_{\text{o}}\right\}^{1/2}, \tag{35}$$

where V_{i} is the initial impact velocity. Note that as $M_{\text{r}} \to \infty$, $\bar{v} \to V_{\text{i}}\, \forall u_{l_{\text{o}}} \in [0, \varepsilon_{\text{D}} l_{\text{o}}]$, which implies that constant velocity compression of the rod is only achieved with a sufficiently large backing mass. A straight-forward order of magnitude argument suggests that $\bar{v} \approx V_{\text{i}}$ when $M_{\text{r}} \geqslant 100$. Substituting for $\bar{v}$ in Eq. (26) gives the dynamic stress immediately behind the 'shock' wave front as

$$\sigma^{\text{d}} = \sigma^{\text{qs}}\left\{1 + 2 \ln(1 - u_{l_{\text{o}}}/(1 + M_{\text{r}})\varepsilon_{\text{D}} l_{\text{o}})\right\} + \rho_{\text{o}} V_{\text{i}}^2/\varepsilon_{\text{D}}. \tag{36}$$

A fourth-order Runge–Kutta numerical scheme can be used to solve Eq. (35) for the displacement of the distal end of the foam rod with time, $u_{l_{\text{o}}}(t)$. Together with Eq. (36) the variation of the dynamic stress σ^{d} with time t can be found. Since the compacted material behind the 'shock' is rigid and at rest, the dynamic stress measured by the pressure bar is also given by Eq. (36). In the limit as $u_{l_{\text{o}}} \to 0$, $\sigma^{\text{qs}} = \sigma_{\text{cr}}^{\text{qs}}$ (the quasi-static plastic collapse stress), the 'shock-enhanced' plastic collapse stress is

$$\sigma_{\text{cr}}^{\text{d}} = \sigma_{\text{cr}}^{\text{qs}} + \rho_{\text{o}} V_{\text{i}}^2/\varepsilon_{\text{D}}. \tag{37}$$

Eq. (37) has also been shown to have relevance for wood (Reid and Peng, 1997) and for aluminium honeycombs (Harrigan et al., 1998a, 1999).

3.2.2. Kinematic existence condition for 'shock' compaction

Assuming that no heat is generated in the specimen, i.e $r = 0$ (Eq. (16)), then it is convenient to introduce the specific free energy (or the Helmholtz free energy) ψ at the common absolute temperature of $\theta^- = \theta^+ = \theta$ defined by (Ericksen, 1991)

$$\psi = U - \theta\eta, \tag{38}$$

where U is the internal energy per unit mass and η the specific entropy. Eliminate U in Eq. (17) with (29) and (38) gives (Ericksen, 1991)

$$[\psi] - (\sigma^- + \sigma^+)[\varepsilon]/2 = \theta([q]/\theta - V_{\text{s}}[\eta])/V_{\text{S}}. \tag{39}$$

Since θ and V_{s} are both positive constants, it follows from Eqs. (18) and (39) that

$$[\psi] \leqslant (\sigma^- + \sigma^+)[\varepsilon]/2. \tag{40}$$

The inequality is a neat expression of the property of the isothermal stress–strain plane illustrated in Fig. 2. The term $(\sigma^- + \sigma^+)[\varepsilon]/2$ is the area under the 'shock' chord between 0 and ε_D, whilst $[\psi]$ is the corresponding area under the stress–strain curve which gives the energy absorbed per unit reference volume of material under quasi-static compression. *Consequently, a greater amount of energy will be expended in the adiabatic 'shock' compaction of a foam rod than in quasi-static compression.* Since $[q/\theta] = 0$, it follows from Eq. (18) that

$$\eta^- \geqslant \eta^+. \tag{41}$$

This implies that an increase in the specific entropy always accompanies the passage of a 'shock'.

Let an element of length Δl be compacted to $\Delta l(1 - \varepsilon_D)$ at the 'shock' front. For an isolated thermodynamic system, the increase in the internal energy of the compacted material can only be due to the loss of the kinetic energy it originally possesses and, therefore, Eq. (33) gives

$$(E_U)_2 - (E_U)_1 = (\sigma^- + \sigma^+)\varepsilon_D \Delta l/2 = \rho_o \bar{v}^2 \Delta l/2. \tag{42}$$

Writing $[\psi] = \sigma^{qs}\,\varepsilon_D$ and multiply Eq. (40) with Δl, substitute for $(E_U)_2 - (E_U)_1$ with Eq. (42), gives

$$\bar{v} \geqslant (2\sigma^{qs}\,\varepsilon_D/\rho_o)^{1/2}. \tag{43}$$

This is the kinematic existence condition for continuing 'steady-shock' wave propagation in the foam rod. Substituting $\sigma^{qs} = \sigma^{qs}_{cr} = C_n\sigma_{ys}(\rho_o/\rho_s)^{3/2}$ (see Part I) into Eq. (43) gives the critical velocity beyond which progressive cell crushing occurs, i.e. exhibiting 'shock'-type characteristics, viz.

$$\bar{v}_{cr} = (2C_n\sigma_{ys}/\rho_s)^{1/2}(\rho_o/\rho_s)^{1/4}\,\varepsilon_D^{1/2}, \tag{44}$$

where subscript $n = 1$ (*small* cell) or 3 (*large* cell). This derivation confirms the result produced by more simplistic arguments by Reid and Peng (1997).

The predicted critical velocity using Eq. (44) is 107.9 and 41.5 ms^{-1} for the *small* (using $\rho_o/\rho_s = 0.101$) and *large* (using $\rho_o/\rho_s = 0.048$) cell foam, respectively. It was shown in Part I that this agrees reasonably well with the experimental values of approximately 100 and 50 ms^{-1}, respectively.

3.2.3. Partitioning of energy absorbed

If strain rate sensitivity of the cell wall material and the compression of trapped gas are negligible, then the difference between the areas under the 'shock' chord and the plastic stress–strain loading path in the interval $[0, \varepsilon_D]$ gives the additional energy absorbed associated with micro-inertial effects. Therefore, the increment of work done, due to micro-inertia, in compacting an increment of thickness δx in the *r-p-p-l* foam rod is

$$\delta W = (\sigma^d - \sigma^{qs})A_o\varepsilon_D\delta x/2. \tag{45}$$

Replacing σ^{d} with Eq. (36) and setting $u_{l_{\mathrm{o}}} = x\varepsilon_{\mathrm{D}}/(1-\varepsilon_{\mathrm{D}})$ in Eq. (45), and integrating from $x = 0$ to $x = l_{\mathrm{o}}$, gives

$$\bar{W} \equiv W/A_{\mathrm{o}}l_{\mathrm{o}} = \rho_{\mathrm{o}}V_{\mathrm{i}}^2/2 + \sigma^{\mathrm{qs}}\varepsilon_{\mathrm{D}} \times \left\{[(1+M_{\mathrm{r}})\varepsilon_{\mathrm{D}} - M_{\mathrm{r}}]\ln\left[1 + \frac{1}{(1+M_{\mathrm{r}})\varepsilon_{\mathrm{D}} - M_{\mathrm{r}}}\right] - 1\right\}. \tag{46}$$

The plastic strain energy density associated with quasi-static compression of the rod is $\sigma^{\mathrm{qs}}\varepsilon_{\mathrm{D}}$; whilst Eq. (46) shows that the energy density associated with inertial effects has a quadratic dependence on the impact velocity for a 'shock-type' compaction process.

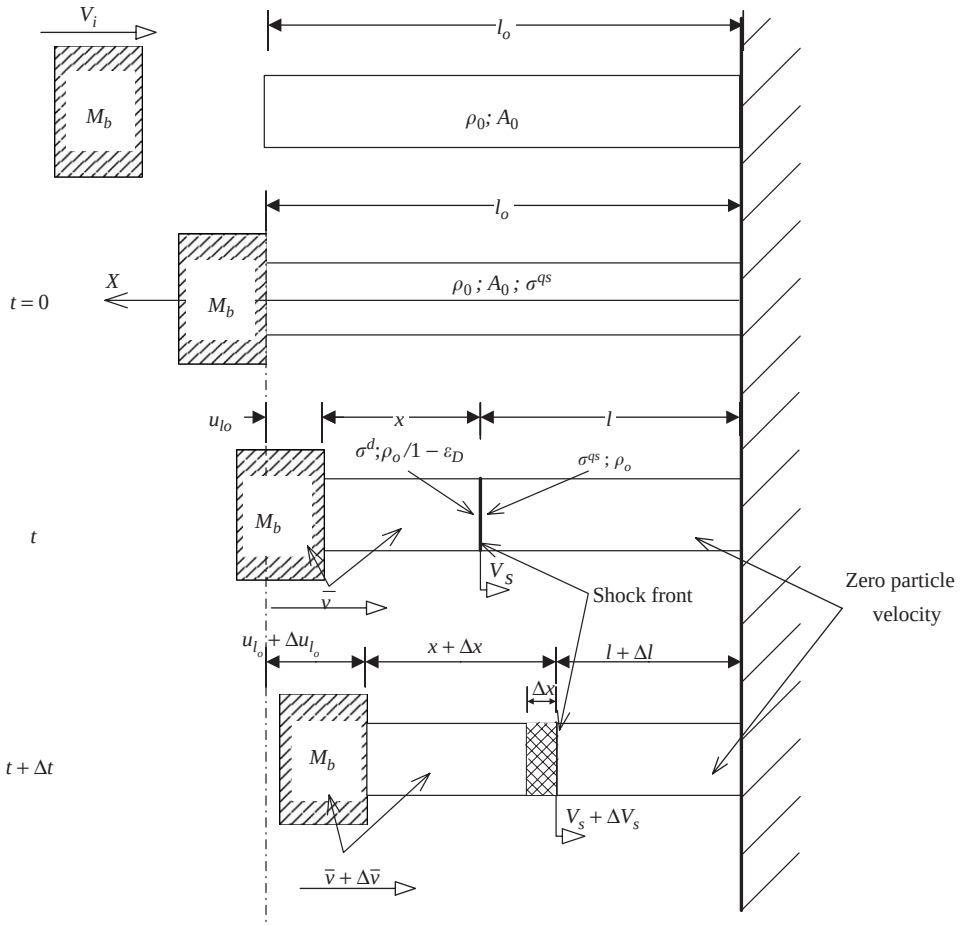

Fig. 6. Parameters defining the 'shock' model for the impact of a rigid mass against a stationary foam rod.

3.3. Impact of a rigid mass against a stationary foam rod

For the sake of completeness, the reverse impact scenario of a rigid mass striking a stationary foam rod is now briefly considered. Suppose a rigid mass M_b travels at a speed of V_i, along the X-axis, until it strikes squarely a foam rod of unit area that is supported at its distal end by the pressure bar, as depicted in Fig. 6. The conditions just ahead and immediately behind the 'shock' front are now as follows:

$$\textit{Behind 'shock' front}: \quad v^- = \bar{v},\ \varepsilon^- = \varepsilon_D,\ \sigma^- = \sigma^d,\ \rho^- = \rho_o/(1-\varepsilon_D) \text{ and} \tag{47}$$

$$\textit{Ahead of 'shock' front}: \quad v^+ = 0,\ \varepsilon^+ = 0,\ \sigma^+ = \sigma^{qs},\ \rho^+ = \rho_o. \tag{48}$$

Note that the 'shock' relation given in Eq. (26) must also apply here. For simplicity, define the scalar variables u_{l_o}, x and l as shown in Fig. 6. From geometry

$$\mathrm{d}l/\mathrm{d}t = -\bar{v}/\varepsilon_D \tag{49}$$

and

$$\mathrm{d}x/\mathrm{d}t = (1-\varepsilon_D)\bar{v}/\varepsilon_D. \tag{50}$$

By Eq. (30), the increase in internal energy of an element Δl in the time interval t and $t+\Delta t$ is

$$\Delta E_U = E_U(t+\Delta t) - E_U(t) = (\sigma^d + \sigma^{qs})\varepsilon_D|\Delta l|/2 \tag{51}$$

and the change in kinetic energy of the agglomerated (crushed) material behind the 'shock' front as it changes velocity from $\bar{v}$ to $\bar{v}+\Delta\bar{v}$ is

$$\Delta E_k = E_k(t+\Delta t) - E_k(t) = M_b\bar{v}\Delta\bar{v} + \frac{\rho_o x\bar{v}\Delta\bar{v}}{(1-\varepsilon_D)} + \frac{\rho_o\bar{v}^2\Delta x}{2(1-\varepsilon_D)} + O(\Delta\bar{v}^2, \Delta\bar{v}\Delta x). \tag{52}$$

Using Eqs. (49)–(52) and neglecting all higher order quantities of small terms, then dividing by Δt and taking the limit $\Delta t \to 0$, Eq. (33) gives

$$(M_r + u_{l_o}/\varepsilon_D l_o)\,\mathrm{d}\bar{v}/\mathrm{d}t = -\sigma_d/\rho_o l_o. \tag{53}$$

Eq. (35) can now be integrated with the initial condition $\bar{v}(u_{l_o}=0) = V_i$ to give the common velocity of the rigid mass and the agglomerated (compacted) material behind the 'shock' as

$$\bar{v} = \left\{\varepsilon_D(M_r^2(\sigma^{qs} + \rho_o V_i^2/\varepsilon_D)/(M_r + u_{l_o}/\varepsilon_D l_o)^2 - \sigma^{qs})/\rho_o\right\}^{1/2}. \tag{54}$$

From Eqs. (26) and (54), the stress immediately behind the 'shock' is

$$\sigma^d = M_r^2(\sigma^{qs} + \rho_o V_i^2/\varepsilon_D)/(M_r + u_{l_o}/\varepsilon_D l_o)^2. \tag{55}$$

4. Discussion

4.1. Comparison with the experimental data

Within the limits of the idealised *r-p-p-l* material model, the predictions of the 'shock' theory compare well with the experimental force-time pulses especially at the higher impact velocities, as is evident in Fig. 7. However, the model does not reliably predict the onset of densification because the actual foam material is not perfectly rigid at its densification strain contrary to the simplified stress–strain curve used. At the lower impact velocities, the experimental force-time pulses are truncated by reflected stress waves. Nonetheless, a reasonable agreement with the experimental pulses is also observed. Similarly, Fig. 8 shows good agreement between the normalised energy absorbed by the foam rod (Fig. 16 of Part I) and the predictions by the 'shock' theory.

The theoretical dynamic plastic collapse stress is given in Eq. (37) and the theoretical dynamic plateau stress is defined as the time average value of $\sigma^{\mathrm{d}}(t)$, Eq. (36), according to (see Part I)

$$\sigma_{\mathrm{pl}}^{\mathrm{d}} = \langle \sigma^{\mathrm{d}} \rangle = \frac{1}{t_{\mathrm{D}}} \int_0^{t_{\mathrm{D}}} \sigma^{\mathrm{d}}(t)\, \mathrm{d}t, \tag{56}$$

where t_{D} corresponds to the time where rigid locking of the whole of the foam specimen has occurred. These are compared with their corresponding experimental

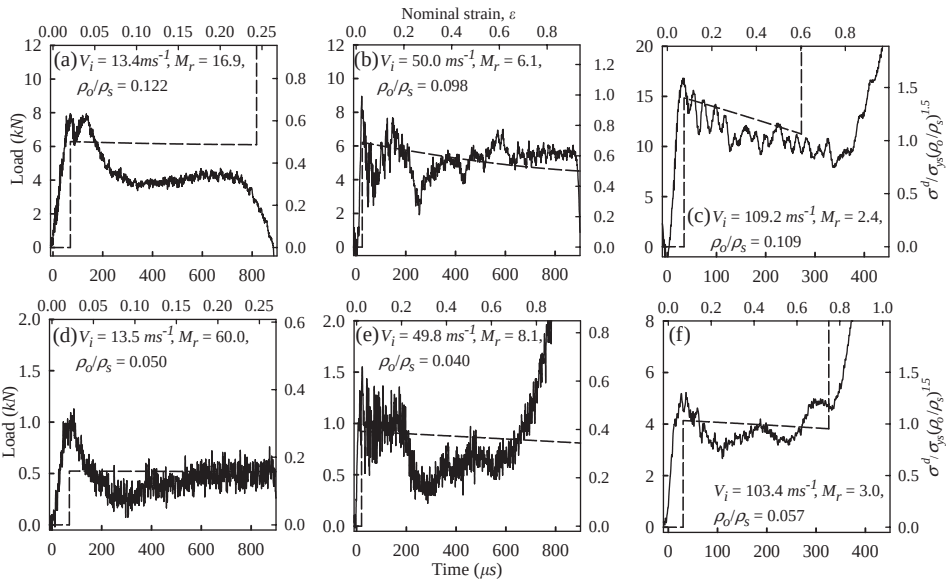

Fig. 7. Comparison between theory (dotted line) and experimental force pulses (solid lines) for *small* (a–c) and *large* (d–f) cell cylindrical *y*-axis specimens measured at different impact velocities V_{i}.

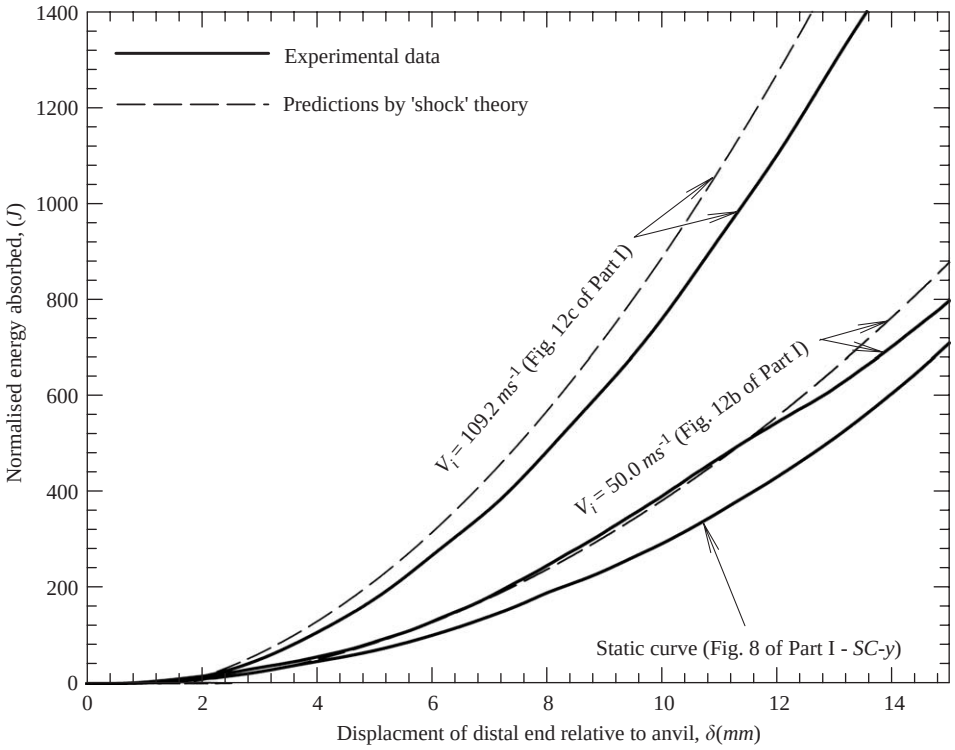

Fig. 8. Comparison between the experimental data for the energy absorbed (normalised by $(\rho_o/\rho_s)^{1.5}$) and the predictions by the 'shock' theory.

values in Figs. 9 and 10. The theoretical predictions for the dynamic plastic collapse stresses, σ_{cr}^{d}, and plateau stresses, σ_{pl}^{d}, agree reasonably well with the experimental data, in particular at the super-critical impact velocities where 'shock' compaction has occurred. The good agreement suggests that the dynamic strength properties at the super-critical velocity regime are affected principally by the impact velocity whilst strength knockdown effects due to the 'size effect' and morphological defects are secondary. Clearly, the 'shock' theory is not applicable in the sub-critical velocity regime because of the different deformation response. Nonetheless, the quadratic trend of the dynamic plastic collapse and plateau stresses with impact velocity is well represented by the theory. In general, the theory appears to provide a better prediction of the strength properties for the *large* cell foam. This is probably because the *large* cell foam's nominal stress–strain curve is better approximated by a perfectly rigid response at its densification strain (locking). The discrepancy between theory and experiment for the *small* cell foam at the higher impact velocities is a result of the higher levels of strain achieved experimentally than are possible analytically when using the simplified material

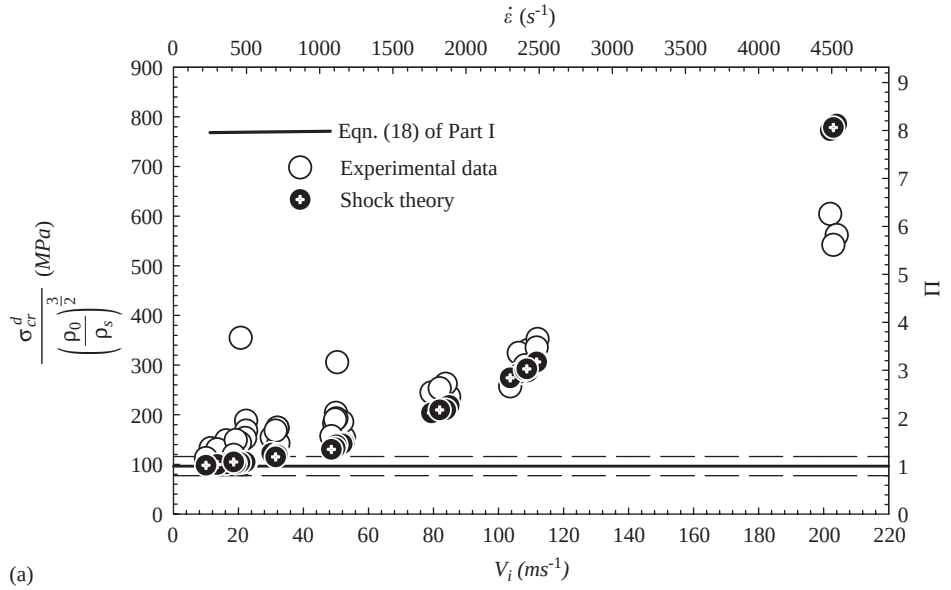

Fig. 9. Comparison between theory and experimental data for the normalised plastic collapse stress $\sigma_{cr}^{d}/(\rho_o/\rho_s)^{1.5}$ of (a) *small* cell and (b) *large* cell *y*-axis specimens. The dashed lines indicate corresponding quasi-static scatter in loads and $\dot{\varepsilon}$ is the nominal engineering strain rate.

model. A greater accuracy could be achieved with the theory presented above by using a more realistic constitutive relationship, such as by Harrigan et al. (2005). This will be pursued elsewhere.

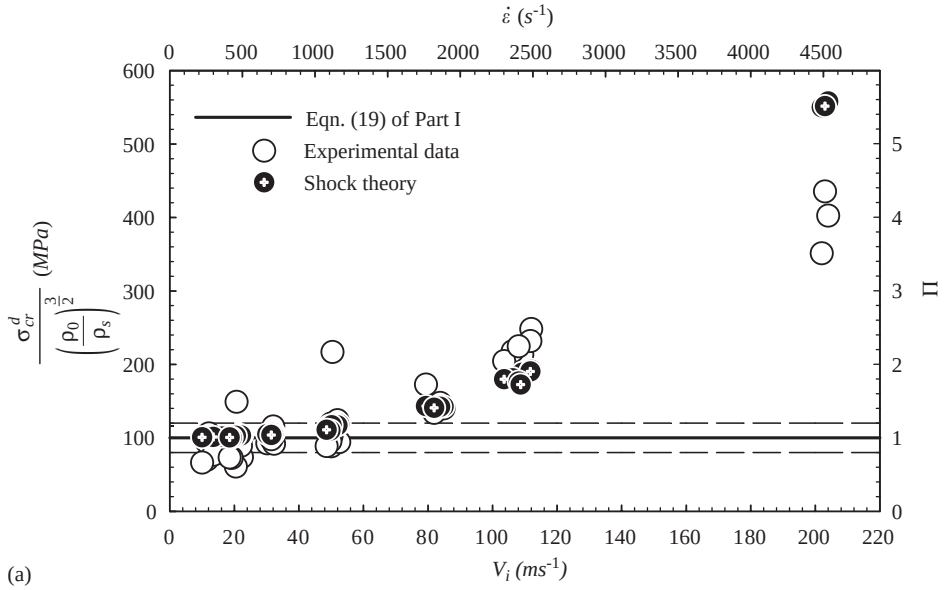

Fig. 10. Comparison between theory and experimental data for the normalised plateau stress $\sigma_{\mathrm{pl}}^{\mathrm{d}}/(\rho_{\mathrm{o}}/\rho_{\mathrm{s}})^{1.5}$ of (a) *small* cell and (b) *large* cell *y*-axis specimens. The dashed lines indicate corresponding quasi-static scatter in loads and $\dot{\varepsilon}$ is the nominal engineering strain rate.

It can be argued, based on extension of the results from studies on 2D regular honeycombs (see Hönig and Stronge, 2002a and b), that dynamic localisation of crushing is not responsible for the significant plastic collapse stress enhancement

observed in the sub-critical velocity regime in Fig. 9. Rather, it is due to the translational and rotational inertia of the cell walls, which is analogous to the lateral inertia effects in Type II structures (Reid et al., 1983). In other words, dynamic strength enhancement is not always an indication of 'shock' propagation per se. This contrasts with the findings of Deshpande and Fleck (2000). In general, the 'shock' theory under-predicts the dynamic plastic collapse stresses of the foams in the sub-critical velocity regime because of the different enhancement mechanism. In contrast, the 'shock' theory tends to over-predict the dynamic plateau stress in this sub-critical velocity regime.

Adiabatic 'shock' compaction of a non-heat-conducting foam rod was assumed to occur in Section 3. In reality, 'shock' changes are not strictly adiabatic; rather, a finite amount of heat energy is generated within the specimen through plastic deformation of the cell walls. The precise nature of the stress–strain relation across the 'shock' at high impact velocities is not known and is most likely to differ somewhat from the adiabatic stress–strain relation used in Eqs. (9) and (23). However, Zaretsky and Ben-Dor (1995) have shown that the adiabatic relation provides a sufficiently good approximation of the 'shock' Hugoniot curve for flexible foams.

For quasi-static compression and dynamic compression in the sub-critical velocity regime there is a characteristic length scale associated with the collapse mechanisms that evolve. Any attempt to use the classical continuum wave theory to model the progression of deformation through aluminium foams in the sub-critical velocity appears futile because of the negative slope in their stress–strain curves, due to local softening associated with the individual cell collapse, and so therefore do not admit wave-type solutions. The difficulties are further complicated by the need to introduce multi-scale effects generated by the cellular geometry. Similarly, there is a characteristic wave thickness associated with the propagating 'shock' front at the super-critical velocities. The thickness of the 'shock' front is the result of a balance struck between dissipative effects and the tendency of the propagating waves to evolve towards a 'shock' due to the rapidly decreasing compressibility of the material (Lighthill, 1956). The dissipative effects are a consequence of the finite time required for cell collapse. The issue concerning the length scales associated with different deformation responses in the transition from a sub-critical velocity regime to a super-critical velocity regime becomes immediately apparent. This will be explored elsewhere.

4.2. Comparison with results of numerical simulations of 2D Voronoi honeycombs

Finite element (ABAQUS Explicit) simulations of simpler 2D Voronoi honeycombs were used to illustrate why a greater expenditure of energy accompanies the 'shock' compaction of cellular solids. Let the minimum Euclidean distance (dist(,)) separating any two neighbouring nuclei, say p_i and p_j, be d_s in the 2D Voronoi honeycomb. If no restriction was previously placed on how the nucleus of each cell is 'seeded' in the plane, then the inequality $dist(p_i, p_j) \geqslant d_s$ must hold for any pair of cell nuclei. Suppose the nuclei are 'seeded' under a constraint that the

Euclidean distance between any pair of neighbouring nuclei must always be equal; then there exists a limiting (maximum) value for d_s given by $d_s^{cr} = (2A/n\sqrt{3})^{1/2}$, where n and A is the number of nuclei and the area of the plane, respectively. A non-dimensional parameter Λ, defined by

$$\Lambda := d_s/d_s^{cr} \quad \text{for} \quad 0 < \Lambda \leqslant 1, \tag{57}$$

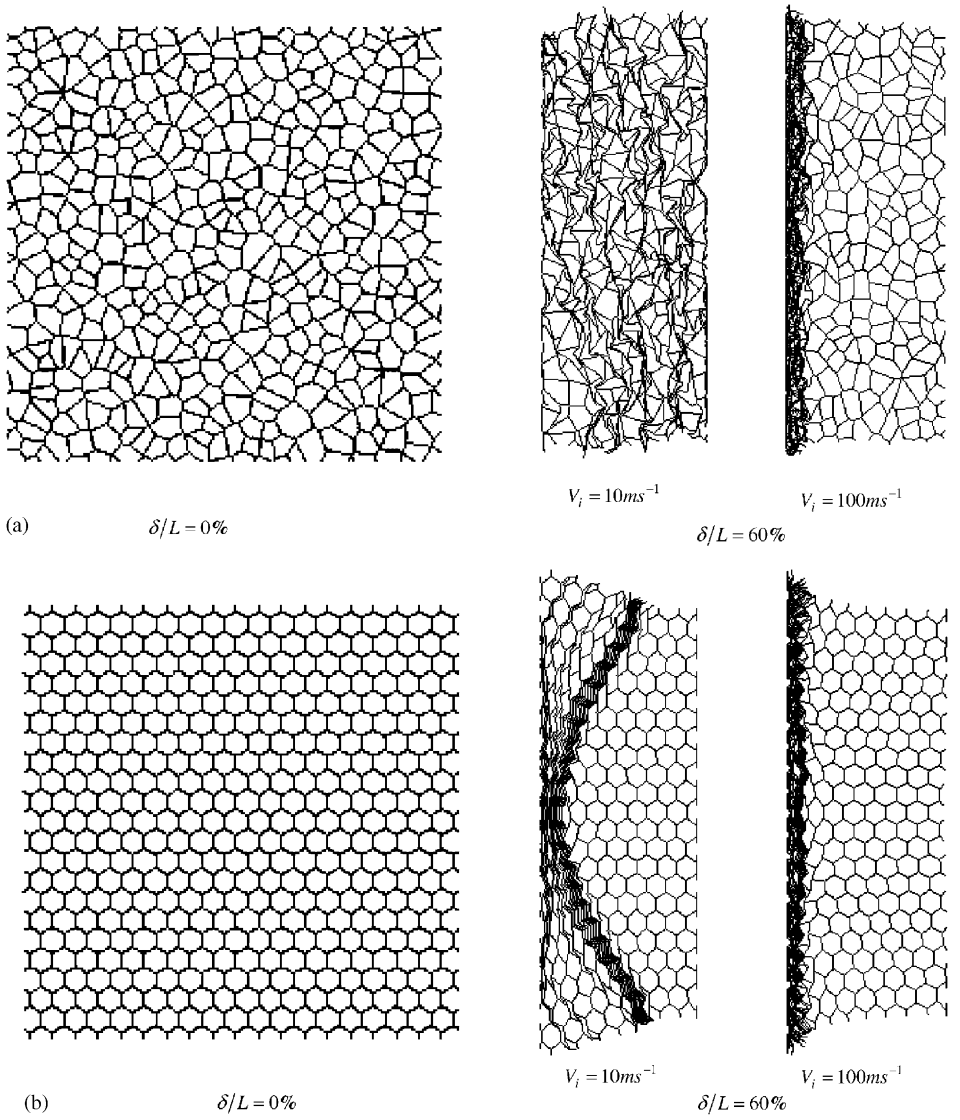

Fig. 11. In-plane compression of 2D Voronoi honeycombs for (a) $\Lambda = 0.5$ and (b) $\Lambda = 1$. Both cases are fixed on their right-end and compressed at a constant velocity from the left-end. The deformed specimens are shown compressed up to 60% of its original length for both velocities.

is used to quantify the extent of cell irregularity in 2D Voronoi honeycombs with the same numbers of nuclei (Zhu et al., 2001). Once the nuclei are seeded, a 2D Voronoi honeycomb is easily generated using the same technique described by Silva et al. (1995). Figs. 11a and b show Voronoi honeycombs for $\Lambda = 0.5$ (~400 cells and 0.32 mm wall thickness) and $\Lambda = 1$ (19×22 regular cells of 4 mm edge length and 0.34 mm wall thickness) respectively. Both have a relative density of 0.1. Their aluminium alloy cell walls have rate-independent, elastic, perfectly-plastic properties identical to those used by Chen et al. (1999). Each cell wall is modelled using 1–15 general-purpose shell elements (S4R) and self-contact simulations have been incorporated. The foams are compressed at constant velocities of $10\,\mathrm{ms}^{-1}$ (sub-critical) and $100\,\mathrm{ms}^{-1}$ (super-critical) from the left, whilst their right-ends remain fixed.

The distribution of crushed cells in the 2D Voronoi honeycombs (Fig. 11) is consistent with those observed in 3D Cymat/Hydro foams (see Part I) in the different velocity regimes. Bands of non-contiguous crushed cells develop at a sub-critical impact velocity; by contrast, sequential cell crushing (or 'shock' wave propagation) occurs at a super-critical impact velocity. Fig. 12 shows the variation of the internal

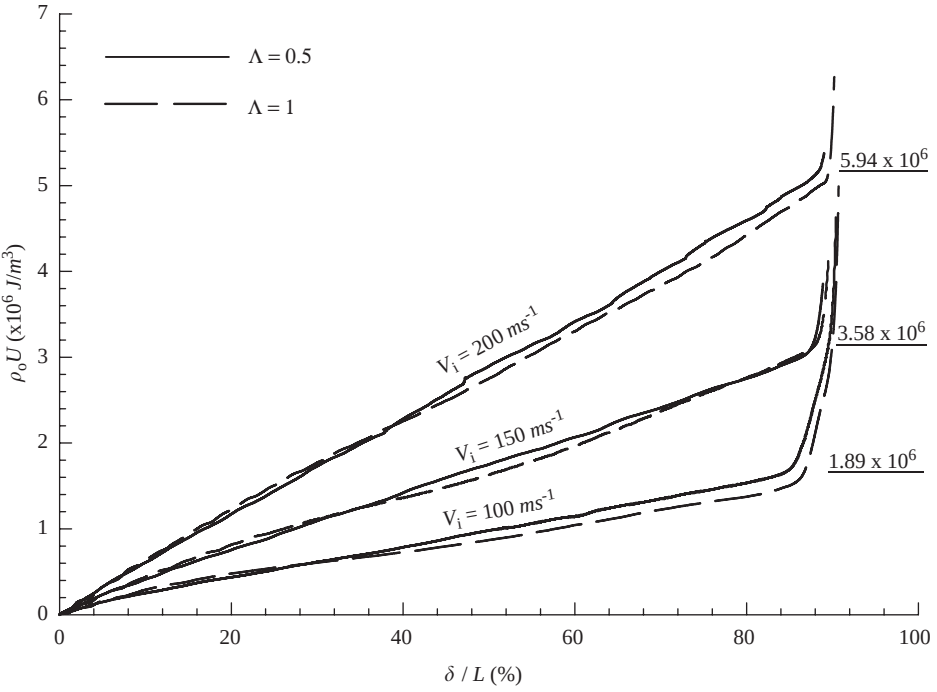

Fig. 12. Internal energy density of 2D Voronoi honeycombs ($\Lambda = 1$ and $\Lambda = 0.5$) versus the normalised displacement (δ/L) at three velocity levels. L is the undeformed specimen length and δ is the displacement of the impact-end of the specimen measured from its initial configuration. The overall energy absorbed at full locking predicted by Eq. (58) for each velocity is given by the underscored values.

energy density (using the identifier 'ALLIE' in ABAQUS) in the Voronoi honeycombs compressed at three super-critical velocities. Since all forms of non-mechanical energies, and the energy dissipated by viscous effects and by time-dependent deformation are not considered in the FE model, the only contributions to the internal energy are the recoverable elastic strain energy and the energy dissipated by plasticity (ABAQUS, 2002). Note that the former is negligibly small. The upturn at the end of each curve indicates an increased absorption of energy by the 2D honeycombs at full locking with impact velocity. It is evident from Fig. 12 that the two key parameters controlling the energy absorption capacity of these honeycombs are their relative density and the impact velocity. By contrast, cell micro-structural irregularities (Λ) had little effect. Zou et al. (2005) have also shown that the energy dissipated through rate-independent plastic deformation in the cell edges occurs mainly in the immediate vicinity ahead of the crush front, and they account for more than 95% of the internal energy density plotted. From Eqs. (19) and (30), it is easily shown that

$$[\rho_o U] = \sigma^+[\varepsilon] + \rho_o[v]^2/2. \tag{58}$$

The predictions by Eq. (58) of the overall energy absorbed at full locking (identified by the upturn in each curve) are given by the under-scored values in Fig. 12. The parameters used in their calculations were $[\varepsilon] = \varepsilon_D = 0.9$, $\sigma^+ = 0.9\,\text{MPa}$ and $[v] = V_i$. The stress ahead of the 'shock' (σ^+) is assumed to be that measured at the fixed-end. It was found to be nearly constant throughout the compression process and varies little with the impact velocity.

The above numerical example show that the increased energy absorbed by the 2D honeycombs (without trapped gas) can be attributed directly to rate-independent plastic deformation in their cell edges caused by the dynamic localisation of crushing, or 'shock' wave propagation. This is an inertial phenomenon wherein microinertia (this term refers to the inertia of the individual cell edges) is expected to play a pivotal role (Reid et al., 1993). Although a full analysis of 3D foams is not yet available, it is expected that the same explanations given above could also be extended to 3D foams under super-critical velocity compression.

4.3. Incorrect global energy balance approach

Consider the case of a 1D end-on impact of a long stationary bar of foam of cross sectional area A by a rigid mass M travelling at an impact velocity V_o (see Fig. 13b). This case was previously analysed by Ashby et al. (2000). The idealised compressive stress–strain curve shown in Fig. 13a was adopted. Their analysis assumes zero particle velocity ahead of the 'shock' and an upstream stress equal to σ_{pl}^{qs}. A global energy balance of the foam energy absorber was given as

$$\frac{1}{2}\left(M + \frac{\rho_o A l}{1-\varepsilon_D}\right)\bar{v}^2 + \sigma_{pl}^{qs}\varepsilon_D \frac{Al}{1-\varepsilon_D} = \frac{1}{2}M_b V_o^2, \tag{59}$$

where l is the current location of the 'shock' front measured from the impact end.

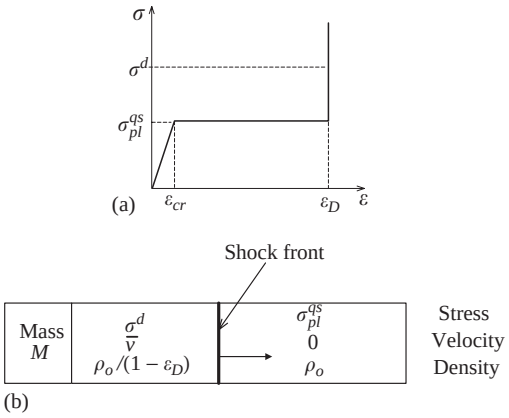

Fig. 13. (a) Schematic compressive stress–strain curve for a metal foam and (b) the stress, velocity on either side of the 'shock' wave front for an impacted foam by a mass M (Ashby et al., 2000).

By comparing terms from Eq. (33), they assert implicitly that the change in internal energy per unit reference area of the bar is

$$(E_{\mathrm{U}})_2 - (E_{\mathrm{U}})_1 = \sigma_{\mathrm{pl}}^{\mathrm{qs}} \varepsilon_{\mathrm{D}} l/(1-\varepsilon_{\mathrm{D}}). \tag{60}$$

Assuming that Eq. (60) is correct, multiplying Eq. (30) with l, and writing $[\rho_{\mathrm{o}} U]l = \sigma_{\mathrm{pl}}^{\mathrm{qs}} \varepsilon_{\mathrm{D}} l/(1-\varepsilon_{\mathrm{D}})$, gives

$$\sigma_{\mathrm{pl}}^{\mathrm{qs}} \varepsilon_{\mathrm{D}} l/(1-\varepsilon_{\mathrm{D}}) - (\sigma^{\mathrm{d}} + \sigma_{\mathrm{pl}}^{\mathrm{qs}}) \varepsilon_{\mathrm{D}} l/2 \neq 0, \tag{61}$$

a contradiction. Thus, by this simple argument, the assertion in Eq. (60) cannot be correct; otherwise, the energy flux is not continuous across the 'shock'. Consequently, Eq. (59) does not account in full for the balance of energy. The results of the numerical example in Fig. 12 clearly show that the change in internal energy across a 'shock' front is dependent upon $[v]$; this contrast with Eq. (60) assumed by Ashby et al. (2000). The correct equation of motion for this case is presented in Section 3.3. It should be noted in passing that similar incorrect application of the global energy balance approach was also made in Lu and Yu (2003).

5. Conclusions

It has been shown that a continuous process of elastic–plastic stress wave propagation into a uniform region in which the mechanical behaviour is represented by a single concave upwards stress–strain relation cannot be maintained indefinitely in a strain-hardening foam rod (Hanssen et al., 2002) and ultimately the plastic wave must show discontinuities, leading to the formation of a 'shock'.

The general quadratic trend of the variation of the dynamic plastic collapse and plateau stresses with impact velocity, evident in the empirical data, is captured well by the simple *r-p-p-l* 1D 'shock' theory. The kinematic existence condition for 'shock' compaction of the foam rod has been established from thermodynamics arguments and it predicts the impact velocity for transition to a 'shock'-type deformation response of approximately $108\,\mathrm{ms}^{-1}$ (small cell foam) and $44\,\mathrm{ms}^{-1}$ (large cell foam) which compares well with the experimental data. The incorrect application of the global energy balance approach to 'shock' propagation in cellular solids in the literature has been highlighted.

Dynamic localisation of crushing is not always responsible for the significant plastic collapse stress enhancement in the sub-critical velocity regime. Rather, this can be due to Type-II micro-inertial effects. Dynamic strength enhancement is not always accompanied by 'shock' propagation per se. Inertial effects associated with the dynamic localisation of crushing are responsible for the enhancement of the dynamic strength properties in the super-critical velocity regime. The predictions of the 'shock' theory compare well with the experiment data in this velocity regime where size effects and morphological defects are insignificant. In the sub-critical velocity regime, both effects influence the dynamic strength properties.

Acknowledgements

This research was supported by the EPSRC under Grant number GR/R26542/01, and by Hydro Aluminium, a.s., through the Norwegian University of Science and Technology (NTNU). The authors wish to thank Professor M. Langseth and Dr. A.G. Hanssen of the Structural Impact Laboratory at NTNU, and Dr. T.Y. Reddy for helpful discussions.

References

ABAQUS Theory Manual, Version 6.3, 2002, HKS Inc., Providence, Rhode Island.

Ashby, M.F., Evans, A.G., Fleck, N.A., Gibson, L.J., Hutchinson, J.W., Wadley, H.N.G., 2000. Metal Foams: A Design Guide. Butterworth Heinemann, Oxford.

Bland, D.R., 1988. Wave Theory and Applications. Oxford University Press, Oxford.

Calladine, C.R., English, R.W., 1984. Strain-rate and inertia effects in the collapse of two types of energy-absorbing structure. Int. J. Mech. Sci. 26, 689–701.

Chen, C., Lu, T.J., Fleck, N.A., 1999. Effect of imperfections on the yielding of two dimensional foams. J. Mech. Phys. Solids 47, 2235–2272.

Deshpande, V.S., Fleck, N.A., 2000. High strain rate compressive behaviour of aluminium alloy foams. Int. J. Impact Eng. 24, 277–298.

Ericksen, J.L., 1991. Introduction to the Thermodynamics of Solids. Chapman and Hall, London.

Eringen, A.C., Şuhubi, E.S., 1974. Elastodynamics. Finite Motions, vol 1. Academic Press, New York.

Hanssen, A.G., Hopperstad, O.S., Langseth, M., Ilstad, H., 2002. Validation of constitutive models applicable to aluminium foams. Int. J. Mech. Sci. 44, 359–406.

Harrigan, J.J., Peng, C., Reid, S.R., 1998a. Inertia effects in impact energy absorbing materials and structures. In: Langseth, M., Krauthammer, T. (Eds.), Transient loading and response of structures,

International Symposium in honour of Arnfinn Jenssen, Trondheim, Norway, ISBN No. 82-7482-044-4, pp. 447–474.

Harrigan, J.J., Reid, S.R., Reddy, T.Y., 1998b. Inertial forces on the crushing of wood loaded along the grain. In: Allison, I.M. (Ed.), Experimental Mechanics. Balkema, Rotterdam, pp. 193–198.

Harrigan, J.J., Reid, S.R., Peng, C., 1999. Inertia effects in impact energy absorbing materials and structures. Int. J. Impact Engng. 22, 955–979.

Harrigan, J.J., Reid, S.R., Tan, P.J., Reddy, T.Y., 2005. High rate crushing of wood along the grain. Int. J. Mech. Sci. 47, 521–544.

Hönig, A., Stronge, W.J., 2002a. In-plane dynamic crushing of honeycomb—Part I: crush band initiation and wave trapping. Int. J. Mech. Sci. 44, 1665–1696.

Hönig, A., Stronge, W.J., 2002b. In-plane dynamic crushing of honeycomb—Part II: application to impact. Int. J. Mech. Sci. 44, 1697–1714.

Hopkins, H.G., 1968. The method of characteristics and its application to the theory of stress waves in solids. In: Heyman, J., Leckie, F.A. (Eds.), Engineering Plasticity. Cambridge University Press, Cambridge, pp. 277–315.

Lighthill, M.J., 1956. Viscosity effects in sound waves of finite amplitude. In: Batchelor, G.K., Davies, R.M. (Eds.), Surveys in Mechanics. Cambridge University Press, Cambridge, pp. 250–351.

Lu, G., Yu, T.X., 2003. Energy Absorption of Structures and Materials. Woodhead Publishing Ltd., Cambridge, UK.

Morland, L.W., 1959. The propagation of plane irrotational stress waves through an elastoplastic medium. Philos. Trans. R. Soc. London A251, 341–383.

Reddy, T.Y., Reid, S.R., Barr, W.W., 1991. Experimental investigation of inertia effects in one-dimensional metal ring systems subjected to end impact—II: free ended systems. Int. J. Impact Eng. 11, 463–480.

Reid, S.R., Bell, W.W., 1984. Response of 1-D metal ring systems to end impact. In: Harding, J. (Ed.), Mechanical Properties at High Rates of Strain. Institute of Physics Conference Series No. 70, Oxford, pp. 471–478.

Reid, S.R., Peng, C., 1997. Dynamic uniaxial crushing of wood. Int. J. Impact Eng. 19, 531–570.

Reid, S.R., Reddy, T.Y., 1983. Experimental investigation of inertia effects in one dimensional metal ring systems subjected to end impact—I: fixed ended systems. Int. J. Impact Eng. 1, 85–106.

Reid, S.R., Bell, W.W., Barr, R.A., 1983. Structural plastic shock model for one dimensional ring system. Int. J. Impact Eng. 1, 175–191.

Reid, S.R., Reddy, T.Y, Peng, C., 1993. Dynamic compression of cellular structures and materials, In: Jones, N., Wierzbicki, T. (Eds.), Structural Crashworthiness and Failure. Elsevier Applied Science Publishers, pp. 295–340.

Silva, M.J., Hayes, W.C., Gibson, L.J., 1995. The effect of non-periodic microstructure on the elastic properties of two-dimensional cellular solids. Int. J. Mech. Sci. 37, 1161–1177.

Tan, P.J., Reid, S.R., Harrigan, J.J., Zou, Z., Li, S., 2005. Dynamic compressive strength properties of aluminium foams. Part 1—Experimental data and observations. J. Mech. Phys. Solids, to appear, doi:10.1016/j.jmps.2005.05.007.

Zaretsky, E., Ben-Dor, G., 1995. Compressive stress–strain relations and shock Hugoniot curves of flexible foams. ASME J. Eng. Mat. Tech. 117, 278–284.

Zhu, H.X., Hobdell, J.R., Windle, A.H., 2001. Effects of cell irregularity on the elastic properties of 2D Voronoi honeycombs. J. Mech. Phys. Solids 49, 857–870.

Zou, Z., Tan, P.J., Reid, S.R., Li, S., Harrigan, J.J., 2005. Dynamic crushing of two-dimensional cellular materials and the effect of irregularities on the crushing behaviour, J. Mech. Phys. Solids, submitted.